Desalination and Water Treatment
www.deswater.com

doi: 10.5004/dwt.2017.20447

67 (2017) 357–370
March

Dodecyl sulfate chain anchored bio-char to sequester triaryl methane dyes: equilibrium, kinetics, and adsorption mechanism

Saikh Mohammad Wabaidur[a], Moonis Ali Khan[a,*], Masoom Raza Siddiqui[a], Zeid Abdullah Alothman[a], Subramanyan Vasudevan[b], Mohammad Saad Al-Gamdi[c], Ibrahim Hotan Al-Sohami[a]

[a]*Chemistry Department, College of Science, King Saud University, Riyadh 11451, Saudi Arabia, emails: moonisalikhan@gmail.com, mokhan@ksu.edu.sa (M.A. Khan), tarabai22@yahoo.com.sg (S.M. Wabaidur), siddiqui124@gmail.com (M.R. Siddiqui), zaothman@ksu.edu.sa (Z.A. Alothman), chem-ihg@hotmail.com (I.H. Al-Sohami)*
[b]*CSIR-Central Electrochemical Research Institute, Karaikudi 630 006, India, email: svasudevan65@gmail.com*
[c]*King Abdulaziz City for Science and Technology (KACST), Riyadh, Saudi Arabia, email: alali311@gmail.com*

Received 24 August 2016; Accepted 16 December 2016

ABSTRACT

A clean and green approach converting waste camel bones to bone bio-char (BC), and its applicability to abate triarylmethane dyes, namely malachite green (MG) and crystal violet (CV), from the aqueous phase was reported. Dodecyl sulfate chain of sodium dodecyl sulfate was anchored over BC (modified camel bone char [MCBC]) surface to enhance its dye sequestering capacity. Adsorption and residual decoloration mechanisms were discussed. Comparatively faster adsorption kinetics for MG than CV was observed. Breakthrough studies revealed profound effect of solution matrix on dyes adsorption. Temkin and Freundlich isotherm models showed better fit for MG and CV adsorption on MCBC, respectively. Thermodynamics study showed spontaneous and endothermic process. The presence of sulfur in elemental analysis and an SO_4^{2-} group peak at 629 cm^{-1} in Fourier transform infrared spectrum confirmed successful MCBC modification. Both MG and CV possess $-N(CH_3)_2^+$ ions and sp^2-hybridized C atoms in their structure. These atoms have a tendency to bind with the –OH group of MCBC through electrostatic interaction/nucleophilic substitution reaction, thus, leading to dyes adsorption. π-electron delocalization results in carbinol derivative formation for both dyes and might be a possible reason for residual dye decoloration with time. Maximum dyes (MG – 45.48% and CV – 44.47%) elutions were observed with acetone and CH_3OH, respectively.

Keywords: Camel bone bio-char; Malachite green; Crystal violet; Sodium dodecyl sulfate; Adsorption mechanism

1. Introduction

Dyes are the complex organic molecules that tend to attach themselves with surfaces or fabrics, imparting desirable colors. More than 100,000 different synthetic dyes are known, with an annual production rate of over 7×10^5 ton/year [1]. Because of their recalcitrant nature, when dyes containing effluents are discharged into water resources, they become a significant source of pollution and pose threats to both aquatic environments and human beings [2]. For sustainable life and water resources, it is important to remove and/or minimize the dye concentration in effluents prior to their being discharged into the natural environment.

Oxidation, adsorption, photocatalysis, and membrane separation are some of the most common techniques used for the abatement of dyes from aqueous medium. Among them, adsorption is considered the most effective process. The low operational cost, minimum sludge production, and applicability even at lower adsorbate concentrations are some of

* Corresponding author.

1944-3994/1944-3986 © 2017 Desalination Publications. All rights reserved.

the major merits of the adsorption process [3]. Activated carbon (AC), a commercially acclaimed adsorbent, was used for the removal of both dyes and heavy metals from wastewater. However, high production and regeneration cost restricts AC's large-scale usage in wastewater treatment. Therefore, it is essential to explore economical and eco-friendly alternate adsorbents for the removal of dyes from aqueous solutions.

Bone bio-char (BC, calcined animal bones) is composed of 9–11 wt% carbon, 70–76 wt% hydroxyapatite (HAP), and 7–9 wt% calcium carbonate. Among them, HAP is the major constituent of BC. Thus, BC represents a source of biogenic apatite, which is a cost-effective alternate to synthetic HAP. Low water solubility, high stability under redox conditions, excellent biocompatibility, chemical stability, and excellent buffering capacity are some of the fundamental properties of HAP. The use of BC for the refining and clarification of cane sugar was reported by Wilson et al. [4]. Since then, it has been extensively used as a biosorbent for decolorizing cane sugar in the sugar industry. The use of HAP and its composites as an adsorbent for the abatement of heavy metals and dyes from wastewater and soil is well reported [5–9].

Dromedary, a one-humped camel (*Camelus dromedarius*), is a major livestock in the Arabian Peninsula, representing 61% of the total camels present in the world [10]. In Saudi Arabia, camel meat constitutes 30% of the meat produced [11]. The carcass comprises 57% muscle, 26% bone, and 17% fat. These bones generate waste, creating waste disposal issues. Therefore, to deal with the waste disposal issue and for a clean and sustainable environment, meaningful utilization of waste camel bones, a natural source of HAP is essential.

Herein, a clean and green approach was engineered to pyrolytically develop BC from waste camel bones, modifying it with comparatively less toxic sodium dodecyl sulfate (SDS). The modification of camel bone bio-char (CBC) with SDS introduces nonpolar moiety (dodecyl) bearing negatively charged sulfate (SO_4^{2-}) ions of SDS by replacing phosphate (PO_4^{3-}) ions present on the CBC surface [12]. Therefore, the hydroxyl group, the end member of HAP, becomes more nucleophilic in the modified adsorbent than the negatively charged SO_4^{2-} group and is consequently substituted by other anions such as fluoride, chloride, or carbonate through electrostatic interaction. The modified adsorbent was termed as modified CBC (MCBC). The applicability of MCBC was tested for the adsorptive removal and consecutive decoloration of Malachite green (MG) and crystal violet (CV) from aqueous solutions.

2. Experimental

2.1. Chemicals and reagents

MG, CV, and SDS were purchased from Sigma-Aldrich Co., USA. Hydrogen peroxide (H_2O_2; 30% w/w in H_2O), hydrochloric acid (HCl), and sodium hydroxide (NaOH) were purchased from Sigma-Aldrich Co., Germany. Methanol (CH_3OH), ethanol (EtOH, C_2H_5OH), acetone (Ace), nitric acid (HNO_3), and sulfuric acid (H_2SO_4) were purchased from BDH Chemicals Co., England. Milli-Q water (Millipore, Bedford, MA, USA) was used throughout the experiments. Other chemicals and reagents used were of analytical reagent grade or as specified.

2.2. Development and modification of CBC

Femur bones of camels (purchased from a local meat shop in Riyadh, Saudi Arabia) were washed with water to remove traces of flesh, fat, and blood. The bones were cut into small pieces and treated with H_2O_2 (30% w/w) to decompose organic content. The treated bones were again washed with water, air-dried, and mechanically grounded. The grounded bones were placed in a crucible and pyrolyzed at 500°C with 10°C/min heating rate in a tubular furnace for 2 h under 100 mL/min nitrogen flow. The pyrolyzed bones were cooled to room temperature in a furnace. The produced CBC was again grounded and passed through 100–200 μm sieve size. Furthermore, CBC was chemically modified with SDS. 200 mL of SDS solutions of varied concentrations (0%–3%) was prepared in 500 mL glass beakers; 2 g of CBC was added in each beaker to make suspensions. The suspensions were aged for 24 h with magnetic stirring under ambient temperature conditions. MCBC samples were filtered and washed several times with ethanol and finally with deionized (D.I.) water to remove unadsorbed SDS traces. The possible schematic CBC modification mechanism is as follows:

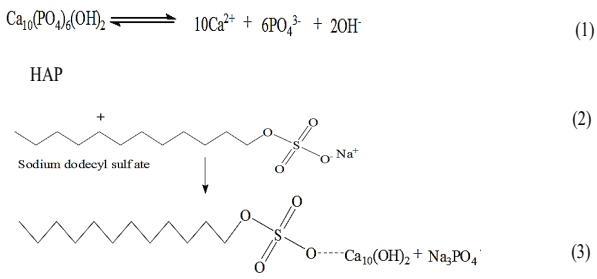

The SDS ions possibly bind with the CBC surface through isomorphous substitution of the PO_4^{3-} ion with the SO_4^{2-} ion and/or due to the electrostatic interaction between SO_4^{2-} and calcium (Ca^{2+}) ions [13]. During modification, a nonpolar dodecyl chain of surfactant was introduced over the CBC surface, possibly decreasing the crystalline nature of MCBC.

2.3. Characterization of MCBC

The surface morphology and elemental content of CBC and MCBC before and after MG and CV adsorption were investigated via scanning electron microscopy (SEM; Nova 200 NanoLab, FEI) coupled with an energy-dispersive X-ray (EDX; AMETEK Nova 200) operated at an accelerating voltage of 30 kV. The functional groups present on the CBC and MCBC surface, actively involved for the binding of dye molecules, were determined by Fourier transform infrared (FT-IR; Thermo Scientific Nicolet 6700 FTIR). The surface area and pore size on MCBC were determined by using an N_2 adsorption/desorption isotherm at 77 K (Micromeritics–Gemini VII 2390 V1.03 surface area analyzer). The surface crystallinity and average particle size of CBC and MCBC were determined via XRD analysis (Philips Xpert XRD).

2.4. Adsorption/desorption experiments

Batch mode adsorption and desorption studies were carried out in 100 mL conical flasks. For adsorption experiments,

25 mL dye solutions of initial concentrations, namely C_0 5–120 mg/L, were equilibrated under ambient temperature conditions for 16 h with 0.05 g MCBC in a temperature-controlled water bath shaker at 100 rpm. At equilibrium, solid/solution phases were separated by using filter paper (Whatman filter paper No. 41), and residual MG and CV were determined by using a UV–visible spectrophotometer (Thermo Scientific Evolution 600, UK) at λ_{max} 618 and 590 nm, respectively. The adsorption capacity (q_e, mg/g) and percentage (%) adsorption were calculated as follows:

$$q_e = (C_o - C_e) \times \frac{V}{m} \quad (4)$$

$$\%\ \text{adsorption} = \frac{C_0 - C_e}{C_o} \times 100 \quad (5)$$

where C_0 and C_e are the initial and equilibrium concentrations of dyes (mg/L), respectively; V is the volume of the adsorbate solution (L); and m is the mass of the adsorbent (g).

To study the effect of pH, experiments were conducted at an initial pH (pH_i) range 2–10. The pH_i was adjusted by the addition of a required amount of 0.1 M HCl and 0.1 M NaOH solution to adsorbate (dye) solutions of C_0 50 mg/L. The adsorption isotherm studies were carried out for the C_0 range 5–120 mg/L at various temperatures. The adsorption kinetics studies were carried out for contact time ranging between 1 and 960 min at varied dye initial concentrations (C_0 25–100 mg/L). The adsorption thermodynamics studies were conducted for temperatures range 293–323 K.

For desorption study, 0.05 g of MCBC samples were initially saturated with 25 mL dye solution of C_0 50 mg/L. The equilibration times for MG and CV were 420 and 960 min, respectively. After saturation, MCBC samples were separated and washed several times using D.I. water to remove unadsorbed traces of dyes. To elute MG and CV, the saturated MCBC samples were treated with 0.1 M NaOH, 0.1 M HCl, 0.1 M HNO_3, 0.1 M H_2SO_4, Ace, CH_3OH, and EtOH for 1,440 min in a water bath shaker under ambient temperature conditions. A control was run to test leaching of the MG and CV ions from the MCBC sample. The concentration of desorbed MG and CV ions were quantitatively analyzed, and percentage desorption was calculated as follows:

$$\%\ \text{desorpton} = \frac{\text{Concentration of dye ions desorbed by eluent}}{\text{Initial concentration of dye ions adsorbed on MCBC}} \times 100 \quad (6)$$

2.5. Breakthrough study

First, 0.5 g of MCBC was put into graduated glass columns with glass wool support. MG and CV solutions of C_0 50 mg/L were prepared in different matrices (such as D.I. water, humic acid [H.A.] and tap water [T.W.]). Then, 600 mL MG and 500 mL CV solutions were passed through columns at 1 mL/min flow rate. The initial 50 mL of the effluent was collected in 10 mL fractions and, thereafter, collected in 50 mL fractions. The residual dyes concentration were quantitatively analyzed.

3. Results and discussion

3.1. Optimizing SDS concentration for CBC modification

CBC was modified with SDS varying its concentration from 0% to 3%. The equilibrium adsorption capacities of MG and CV were increased from 11.83 to 24.93 mg/g and 9.43 to 21.84 mg/g, respectively, with an increase in SDS concentration from 0% to 2% (Fig. 1). Further increase in SDS concentration (above 2%) showed a decrease in MG and CV adsorption. The electrostatic interactions responsible for binding the $(CH_3)_2N^+$– group of dyes with the negatively charged SO_4^{2-} ion head of SDS decreased due to the increase in hydrophobic interaction of both dyes with nonpolar moiety of the SDS, resulting in a red shift of the λ_{max} values of dyes, consequently decreasing the dye binding capacity [13]. Therefore, 2% SDS concentration was optimized for CBC modification.

3.2. Effect of pH

The adsorption of MG and CV on MCBC as a function of pH was isothermally examined. Under highly acidic conditions (i.e., initial pH (pH_i) 2–3), no adsorption of MG and CV on MCBC was observed (Fig. 2). At pH_i 3.14, the adsorption of MG was 24.53 mg/g. Further increase in pH_i from 3.14 to 9.45 yielded a very slow increase in MG adsorption. Maximum MG adsorption (24.94 mg/g) on MCBC was observed at pH_i 9.45. The adsorption of CV on MCBC increased from 18.46 to 20.83 mg/g as pH_i increased from 3.97 to 6.31, attaining the maximum (22.35 mg/g) value at pH_i 9.57. The observed point of zero charge (pH_{PZC}) of MCBC was ~8.1. The adsorption of both dyes on MCBC moved the final pH (pH_f) values toward pH_{PZC} values (Fig. 3), thus revealing the excellent buffering properties of MCBC [14]. The buffering characteristics of MCBC are due to the acid–base reactions of the

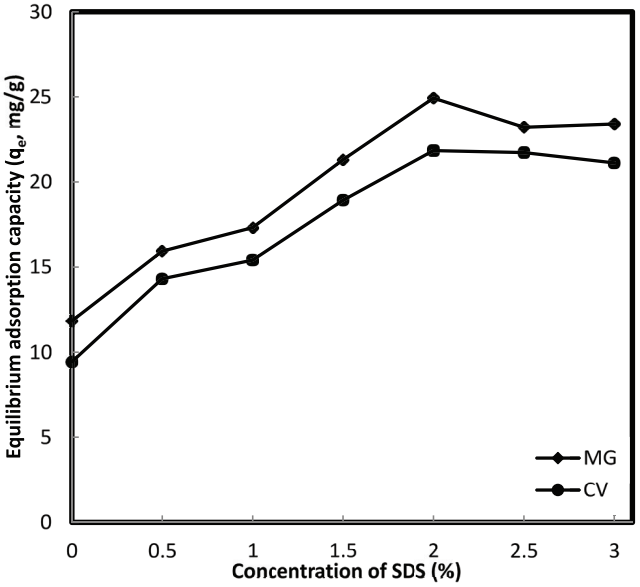

Fig. 1. Effect of SDS concentration on MG and CV adsorption onto CBC (conditions: m – 0.05 g, V – 0.025 L, T – 293 K, contact time – 1,440 min, agitation speed – 100 rpm, C_0^{MG} – 50 mg/L, C_0^{CV} – 50 mg/L).

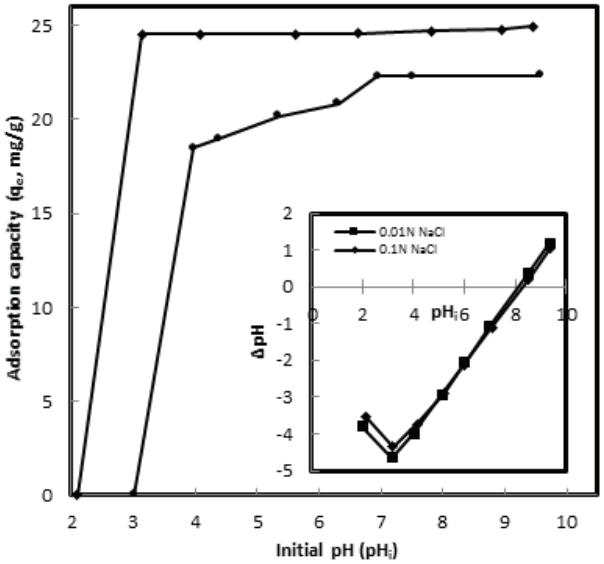

Fig. 2. Effect of pH_i on MG and CV adsorption onto MCBC (inset: pH_{PZC} plot of MCBC; conditions: m – 0.05 g, V – 0.025 L, T – 293 K, contact time – 720 min for CV [●] and 360 min for MG [♦], agitation speed – 100 rpm).

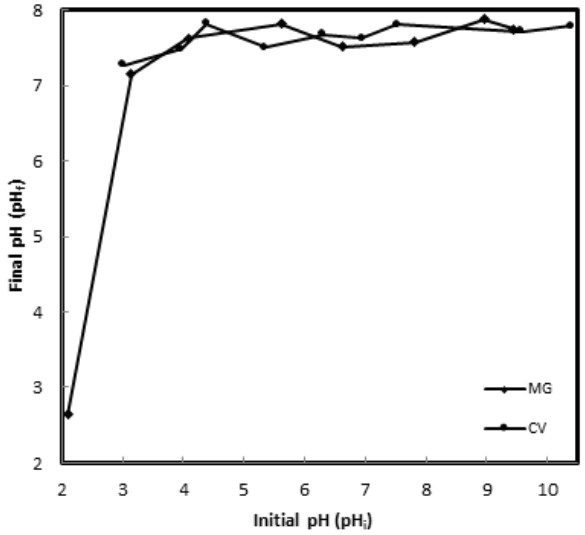

Fig. 3. Plot showing variation in pH after MG and CV adsorption on MCBC.

reactive sites [15]. Compositionally, BC contains 70%–76% HAP [$Ca_{10}(PO_4)_6(OH)_2$]. The modification of CBC with SDS introduced SO_4^{2-} ions over the MCBC surface by exchanging most of the PO_4^{3-} ions. Hence, the possible reactions of MCBC in the aqueous phase are:

$$\equiv SO + H^+ \leftrightarrow \equiv SOH^0 \quad (7)$$

$$\equiv PO^- + H^+ \leftrightarrow \equiv POH^0 \quad (8)$$

$$-Ca(OH)-OH_2^+ \leftrightarrow -Ca(OH)-OH + H^+ \quad (9)$$

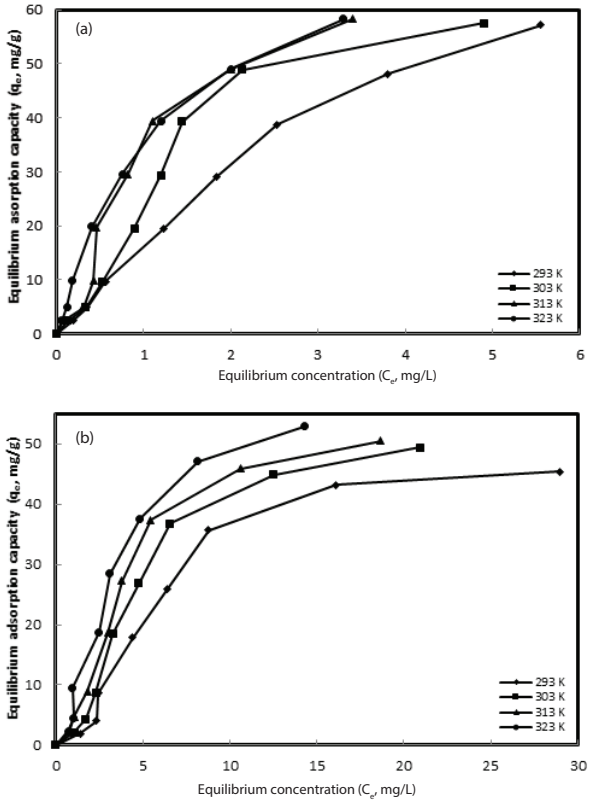

Fig. 4. Effect of concentration on MG (a), and CV (b) adsorption at varied temperatures onto MCBC.

Under acidic conditions (below pH_{PZC}), the consumption of protons from the solution during protonation of the MCBC surface results in an increase in pH_f, whereas under basic conditions (above pH_{PZC}), a decrease in pH_f due to hydroxyl (OH^-) ions consumption via deprotonation of the surface takes place. Thus, the neutral charged species predominates in an alkaline medium, causing the MCBC surface to become negatively charged in an alkaline solution. Therefore, the adsorption of MG and CV on MCBC increases as the pH_i of the solution increases.

3.3. Effect of concentration and adsorption isotherms

Figs. 4(a) and (b) illustrate the effect of the initial concentration of MG and CV for the adsorption on MCBC at varied temperatures. The results indicate that the adsorption capacities of MG and CV increase with increasing initial adsorbate concentration (C_0 5–120 mg/L) and reaction temperature (T 293–323 K). This is due to an increase in MG and CV concentration gradient with concentration, which serves as a driving force during the adsorption process. Additionally, the increase in reaction temperature causes a change in MCBC pore size, increases MG and CV dye ions kinetic energy in the aqueous phase, and enhances the MG and CV dye ions intraparticle diffusion rate [16]. At 293 K, the adsorption capacity of MG varies between 2.40 and 57.22 mg/g, while the adsorption capacity of CV varies between 1.94 and 45.33 mg/g. At 303 K, the MG adsorption

capacity varies between 2.43 and 57.55 mg/g, while the CV adsorption capacity varies between 2.11 and 49.34 mg/g. At 313 K, the MG uptake varies between 2.46 and 58.30 mg/g, while the CV uptake varies between 2.26 and 50.47 mg/g. At 323 K, the MG adsorption varies between 2.47 and 58.35 mg/g, while the adsorption of CV varies between 2.29 and 52.86 mg/g. For the studied temperature and concentration range, the MG adsorption capacity is comparatively higher than that of CV. A smaller molecular volume for MG (220.2 cm^3/mol) compared with CV (291.2 cm^3/mol) might be a possible reason [17]. Because of the smaller molecular volume, MG provides less steric hindrance effect, leading to stronger diffusion ability and the occupation of a smaller space on the MCBC surface compared with CV.

The adsorption data were modeled by using two parameter adsorption isotherm models, namely Langmuir, Freundlich, and Temkin. Langmuir model assumes formation of monolayer during adsorption process without any interaction between adsorbed molecules, in linearized form expressed as [18]:

$$\frac{C_e}{q_e}=\frac{1}{K_L q_m}+\frac{1}{q_m}\times C_e \tag{10}$$

where K_L (L/mg) and q_m (mg/g) are the Langmuir constants related to heat of biosorption and maximum solid phase (i.e., dye) loading on MCBC, respectively.

The essential feature of Langmuir isotherm was determined by a dimensionless constant, separation factor (R_L), can be expressed as:

$$R_L=\frac{1}{1+K_L C_o} \tag{11}$$

If $R_L > 1$ (unfavorable adsorption), $0 < R_L < 1$ (favorable adsorption), $R_L = 1$ (linear adsorption), $R_L = 0$ (irreversible adsorption).

Freundlich isotherm is an empirical expression and assumes that adsorption occurs on the heterogeneous surface sites, in linearized form expressed as [19]:

$$\log q_e=\log K_F+\frac{1}{n}\log C_e \tag{12}$$

where K_F [(mg/g)(L/mg)$^{1/n}$] and n are the Freundlich constants. The Freundlich constant n represents deviation in adsorption from linearity. If $n = 1$ (linear adsorption process), $n < 1$ (chemical adsorption process), $n > 1$ (physical adsorption process).

Temkin isotherm assumes that during adsorption process the adsorption energy decreases linearly. Temkin isotherm contains a factor that explicitly takes into account the adsorbate species–adsorbent interactions [20], in linearized form expressed as:

$$q_e=B_T \ln K_T+B_T \ln C_e \tag{13}$$

where $B_T = RT/b$; R is the universal gas constant (8.314 J/mol K); T is the absolute temperature (K); b is a Temkin constant related to the adsorption energy (kJ/mol); and K_T is the binding constant at equilibrium corresponding to the maximum binding energy (L/g).

It was found that the adsorption of MG on MCBC at various reaction temperatures fit the Temkin model, as depicted for higher regression coefficient (r^2) values, while the adsorption of CV on MCBC at various reaction temperatures obeyed the Freundlich model (Table 1). The values of K_T for MG adsorption on MCBC increased with increasing temperature, showing an increase in adsorbate–adsorbent binding interaction with temperature. The values of Freundlich constant n for MG were in the range of physical adsorption, while for CV adsorption on MCBC at various temperatures, the values were in the range of chemical adsorption. The values of the separation factor (R_L) for the adsorption of MG and CV were in the range of favorable adsorption. Previous studies for

Table 1
Isotherm parameters for the adsorption of MG and CV on MCBC

Isotherm model	MG				CV			
	293 K	303 K	313 K	323 K	293 K	303 K	313 K	323 K
Langmuir								
$q_{m,exp}$ (mg/g)	57.22	57.55	58.30	58.35	45.33	49.34	50.47	52.86
$q_{m,cal}$ (mg/g)	0.01	0.02	0.03	0.01	67.57	85.47	81.97	80
K_L (L/mg)	19.04	40.22	347.25	55.52	0.0849	0.0768	0.1007	0.1526
R_L	0.0004	0.0002	0.00002	0.00015	0.0894	0.0979	0.0764	0.0518
r^2	0.4618	0.2785	0.1488	0.9339	0.8966	0.7385	0.8055	0.9522
Freundlich								
K_F [(mg/g)(L/mg)$^{1/n}$]	14.148	22.029	32.832	38.976	1.799	2.010	3.717	4.225
n	1.0451	1.0863	1.0391	1.0611	0.765	0.608	0.700	0.656
r^2	0.9806	0.9834	0.9704	0.9758	0.9025	0.9792	0.9982	0.9814
Temkin								
B_T	25.23	20.30	19.50	16.34	12.20	16.77	17.54	15.75
K_T (L/mg)	1.763	3.345	6.076	9.575	1.702	1.063	1.345	0.303
r^2	0.9984	0.9882	0.9901	0.9907	0.8683	0.9783	0.9814	0.8745

MG and CV adsorption on various adsorbents reported the applicability of both the Langmuir and Freundlich models (Table 2) [21–28].

3.4. Effect of contact time and adsorption kinetics

A contact time study for the adsorption of MG and CV on MCBC was carried out for the concentration range C_0 25–100 mg/L. Initially, faster MG and CV adsorption rates, due to abundantly available free binding sites on the MCBC surface, were observed, gradually slowing as time elapsed due to the saturation of active binding sites and finally attaining equilibrium. The MG equilibration time for the specified concentration range varied between 240 and 360 min (Fig. 5(a)), while the CV equilibration time for the studied concentration range varied between 600 and 720 min (Fig. 5(b)). During the study, for the assigned concentration range, 72%–85% of MG and 20%–67% of CV was adsorbed within 60 min, showing comparatively faster adsorption kinetics for MG.

The kinetic studies predicted the progress of adsorption; however, the determination of the adsorption mechanism is also important for design purposes. In this investigation, pseudo-first-order and pseudo-second-order kinetics models were tested. Pseudo-first-order kinetics model assumes

Table 2
Summary of MG and CV adsorption results along with their experimental conditions

Adsorbent/ adsorbate	Experimental conditions	Isotherm model applicable	Kinetics		Thermodynamics	Reference
			Equilibration time (min)	Model applicable		
Egg shells/CV	m – 30 g/L; C_0 – 20–100 mg/L; agitation speed – 150 rpm, T – 293 K, contact time – 4 h	Langmuir	240	Pseudo-second-order	Exothermic	[21]
(a) Jute fiber carbon/MG and (b) Jute fiber carbon/CV	For both (a) and (b): m – 0.05 g; pH – 8; agitation speed – 150 rpm; T – 30°C	Freundlich isotherm for both (a) and (b)	(a) 220 and (b) 150	Pseudo-second-order	Endothermic	[22]
Prosopis cineraria sawdust/MG	m – 0.4 g; pH – 6 – 10; agitation speed – 160 rpm; T – 27°C	–	30–45	Pseudo-first-order	Endothermic	[23]
Azadirachta indica sawdust/MG	pH – 7.2; T – 30°C; agitation speed – 100 rpm	Langmuir	14	Pseudo-first-order	Exothermic	[24]
Rattan sawdust/ MG	m – 0.3 g; pH – 10; T – 30°C; agitation speed – 130 rpm	Langmuir	210	Pseudo-first-order	Endothermic	[25]
Tomato paste waste carbon/CV	C_0 – 20–350 m/L; m – 0.1 g; T – 25°C; pH – 8; agitation speed – 120 rpm	Freundlich	150	Pseudo-second-order	Endothermic	[26]
Ginger waste/MG	m – 0.05 g; pH – 9, T – 50°C	Freundlich/ Langmuir	150	Pseudo-second-order	Endothermic	[27]
(a) Red mud/MG and (b) Red mud/ CV	For both (a) and (b): m – 0.25 g; pH – 7; T – 25°C, agitation speed – 180 rpm	Langmuir	(a) 90 and (b) 180	Pseudo-second-order	(a) Endothermic and (b) exothermic	[17]
Grapefruit peel/ CV	m – 1 g/L, pH – 6, T – 45°C; agitation speed – 100 rpm	Langmuir	60	Pseudo-second-order	Endothermic	[28]
(a) MCBC/MG and (b) MCBC/CV	m – 0.05 g; pH – 7, T – 20°C; agitation speed – 100 rpm, C_0 – 5–120 mg/L	(a) Temkin and (b) Freundlich	(a) 240–360 and (b) 600–720	(a) Pseudo-second-order and (b) pseudo-first-order (at lower concentration) and pseudo-second-order (at higher concentration)	Endothermic	Present study

that the adsorption is controlled by diffusion stage, and the adsorption rate corresponds to the difference between equilibrium adsorption capacity and adsorbed quantity at time *t*. Model in linearized form is given as [29]:

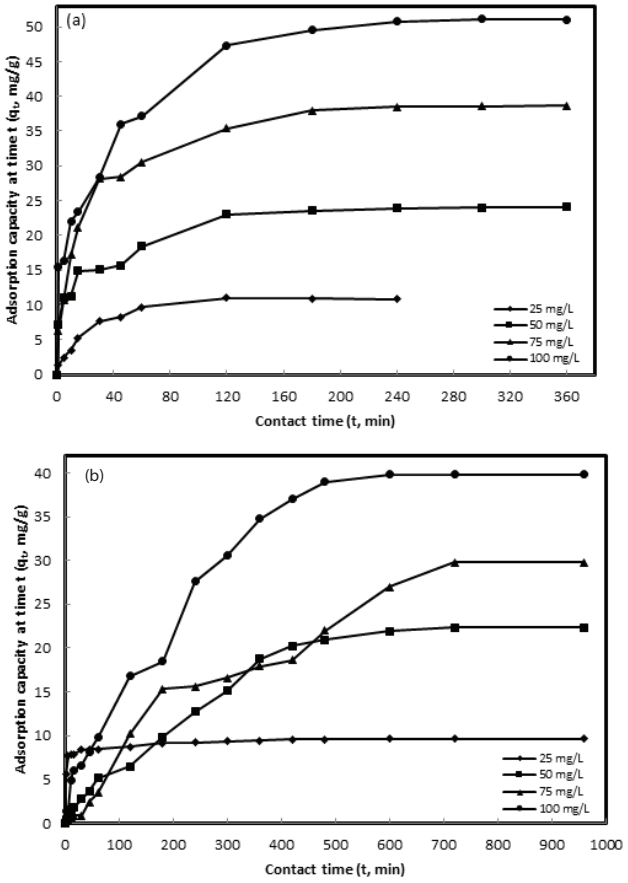

Fig. 5. Effect of contact time on MG (a), and CV (b) adsorption at varied concentrations onto MCBC.

$$\log(q_e - q_t) = \log q_e - \frac{K_1}{2.303} \times t \tag{14}$$

where q_e and q_t (mg/g) are the adsorption capacities at equilibrium and at time *t*, respectively; K_1 (1/min) is pseudo-first-order rate constant.

The rate of adsorption during pseudo-second-order model is controlled by chemisorption mechanism, which includes sharing or transferring of electrons between the interfaces. Pseudo-second-order model [30], in linearized form, is expressed as:

$$\frac{t}{q_t} = \frac{1}{h} + \frac{1}{q_e} \times t \tag{15}$$

$$h = K_2 q_e^2 \tag{16}$$

where *h* (mg/g min) is initial sorption rate; K_2 (g/mg min) is the pseudo-second-order rate constant.

The results show that the adsorption of MG on MCBC at various concentrations followed the pseudo-second-order kinetics model, as depicted by the higher regression coefficient (r^2; Table 3). Additionally, the applicability of the model was proven by nearer $q_{e,\exp}$ and $q_{e,\text{cal}}$ values. The adsorption of CV at 25 mg/L obeyed the pseudo-second-order model, while at higher concentrations, namely C_0 50–100 mg/L, the pseudo-first-order model was applicable. The results agreed well with previously reported results (Table 2). Moreover, the values of *h* for MG were higher compared with those for CV, showing the comparatively faster MG removal rate [31].

3.5. Adsorption thermodynamics

The adsorption thermodynamics parameters, such as standard enthalpy change ($\Delta H°$) and standard entropy change ($\Delta S°$), for the adsorption of MG and CV on MCBC

Table 3
Kinetics parameters for the adsorption of MG and CV on MCBC

Kinetics model	MG				CV			
	C_0 (mg/L)				C_0 (mg/L)			
	25	50	75	100	25	50	75	100
$q_{e,\exp}$ (mg/g)	10.89	24.10	38.64	51.11	9.66	22.32	29.75	39.81
Pseudo-first-order								
$q_{e,\text{cal}}$ (mg/g)	9.20	15.12	13.87	38.25	2.16	26.74	31.02	59.13
K_1 (1/min)	0.0180	0.0186	0.0198	0.0193	0.0074	0.0060	0.0032	0.0094
r^2	0.9838	0.9905	0.9912	0.9929	0.9508	0.9441	0.9246	0.8522
Pseudo-second-order								
$q_{e,\text{cal}}$ (mg/g)	11.57	25.06	40.32	53.76	9.61	30.12	49.02	48.54
K_2 (g/mg min)	0.0056	0.0030	0.0018	0.0011	0.0196	0.0001	0.00003	0.00012
h (mg/g min)	0.7501	1.8843	2.9265	3.1795	1.8118	0.0907	0.0721	0.2827
r^2	0.9984	0.9956	0.9987	0.9955	0.9995	0.7827	0.4105	0.8389

Table 4
Thermodynamics parameters for the adsorption of MG and CV on MCBC

C_0 (mg/L)	MG						CV					
	ΔS° (J/mol K)	ΔH° (kJ/mol)	(–) ΔG° (kJ/mol)				ΔS° (kJ/mol K)	ΔH° (kJ/mol)	(–) ΔG° (kJ/mol)			
			293 K	303 K	313 K	323 K			298 K	308 K	318 K	328 K
5	133.42	31.217	7.872	9.128	10.738	11.773	87.338	23.041	2,452.57	3,444.93	4,579.76	4,959.71
20	124.33	28.226	8.640	9.073	9.974	12.578	102.451	25.632	4,742.65	5,082.87	5,912.12	7,954.49
60	113.01	24.545	8.412	9.804	11.134	11.701	88.303	20.733	5,087.59	6,093.55	6,935.34	7,741.80
100	84.11	16.386	7.868	9.643	10.121	10.499	80.750	19.562	4,087.12	4,966.24	5,614.94	6,565.32

were evaluated by using a Von 't Hoff's plot (between $\ln K_c$ and $1/T$). The Von 't Hoff equation is given as:

$$lnK_c = \frac{\Delta S^\circ}{R} - \frac{\Delta H^\circ}{R} \times \frac{1}{T} \quad (17)$$

where K_c is an equilibrium constant; R is the universal gas constant (8.314 J/mol K); and T (K) is the absolute temperature.

The values of the equilibrium constant (K_c) were calculated as:

$$K_c = \frac{C_{Ae}}{C_e} \quad (18)$$

where C_{Ae} (mg/L) and C_e (mg/L) are the concentrations at equilibrium of the adsorbate on the solid (adsorbent) phase and in the aqueous phase, respectively.

The standard free energy change (ΔG°) was calculated as:

$$\Delta G^\circ = -RTlnK_c \quad (19)$$

The results are presented in Table 4. From the results, it was found that the positive ΔH° values at various MG and CV concentrations (C_0 5–100 mg/L) confirmed the endothermic nature of adsorption. The observed results are consistent with those reported in the literature (Table 2), where both the endothermic and exothermic nature of the CV and MG adsorption process for various adsorbents were reported. The adsorption of MG and CV on MCBC at various concentrations was spontaneous at the temperatures under investigation (298–328 K), as indicated by the negative ΔG° values, and the spontaneity increased with increasing reaction temperature. Randomness at the solid/solution interface during the adsorption process was confirmed by the negative ΔS° values.

3.6. Breakthrough studies

H.A., together with fulvic acid (F.A.), is the core of all humic substances of natural organic matters in water resources, while T.W. contains many ions (such as Ca^{2+}, Mg^{2+}, Cl^-, and SO_4^{2-}) generally present in wastewater [32]. Therefore, it is essential to test the adsorptive performance of MCBC for MG and CV removal in the presence of these counter ions because these ions are generally present under different aquatic environmental conditions. Therefore, the breakthrough and exhaustive capacities of MCBC for MG and CV adsorption were evaluated in D.I. water, H.A., and T.W. matrices. A dye (MG and CV) solution of C_0 50 mg/L was prepared in the aforementioned matrices. The concentration of H.A. used as a matrix for MG and CV solutions was 30 mg/L because this concentration of H.A. generally exists in surface waters [33]. For MG, 20 mL of the effluent was passed through the column without detecting MG when D.I. water was used as a matrix, while 10 mL of each effluent was passed through the column without detecting MG when H.A. and T.W. were used as the matrices (Fig. 6(a)). The breakthrough capacities for MG in D.I. water, H.A., and T.W. matrices were 2, 1, and 1 mg/g, respectively, while the exhaustive capacities were 50, 45, and 27.5 mg/g, respectively. For CV, 20 mL of each effluent was passed through the column without detecting CV when D.I. water and H.A. were used as matrices, whereas 10 mL of effluent was passed when T.W. was used as the matrix (Fig. 6(b)). The breakthrough capacities in D.I. water, H.A., and T.W. matrices were 2, 2, and 1 mg/g, respectively, and the exhaustive capacities were 47.5, 30, and 35 mg/g, respectively.

3.7. Desorption studies

Various acids (HCl, HNO_3, and H_2SO_4) and a base (NaOH) with a concentration of 0.1 M and solvents (Ace, CH_3OH, and EtOH) were tested to elute MG and CV from MCBC. To verify the leaching of adsorbed dyes from MCBC, a control experiment was also run. Dye (MG and CV) solutions of C_0 50 mg/L were adsorbed on the MCBC. At equilibrium, solid/solution phases were separated, and residual dye concentrations were measured. The percentage adsorption of MG varied between 88.5% and 89.7%, while for CV, the percentage adsorption varied between 91.76% and 91.96%. To remove the unadsorbed MG and CV traces, the saturated MCBC samples were washed several times using D.I. water. Furthermore, MCBC samples were treated with various eluents for 24 h. Control experiments showed that 0.501% and 0.283% of MG and CV leached out, respectively. Desorption of MG from MCBC was negligible when the acids and base were used as eluents. The maximum (45.48%) amount of MG was eluted out using Ace (Fig. 7(a)). A trace amount of CV was desorbed using the acids and base. The maximum (44.47%) amount of CV was eluted out using CH_3OH (Fig. 7(b)). The maximum elution of MG and CV from the MCBC surface by Ace and CH_3OH strongly

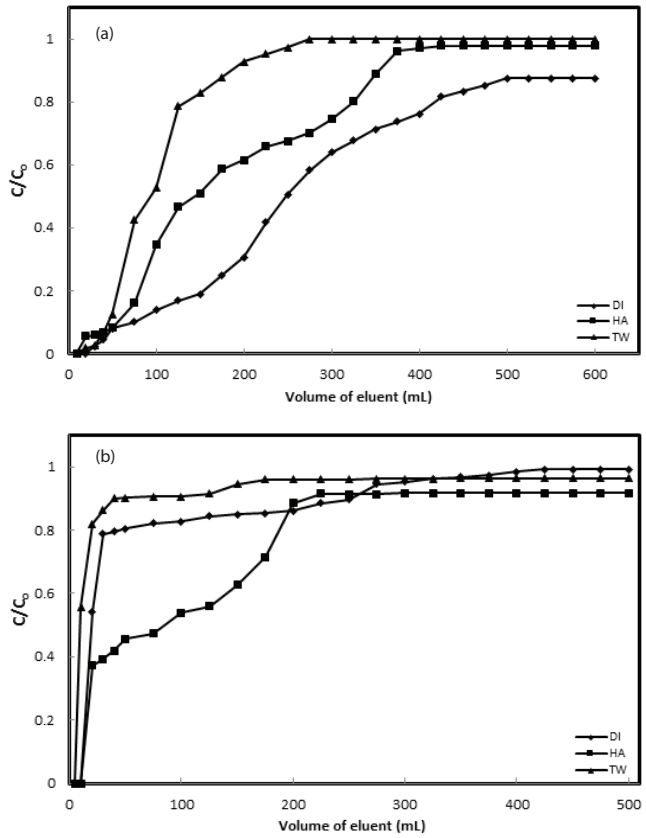

Fig. 6. Breakthrough plots for the adsorption of MG (a) and CV (b) on MCBC.

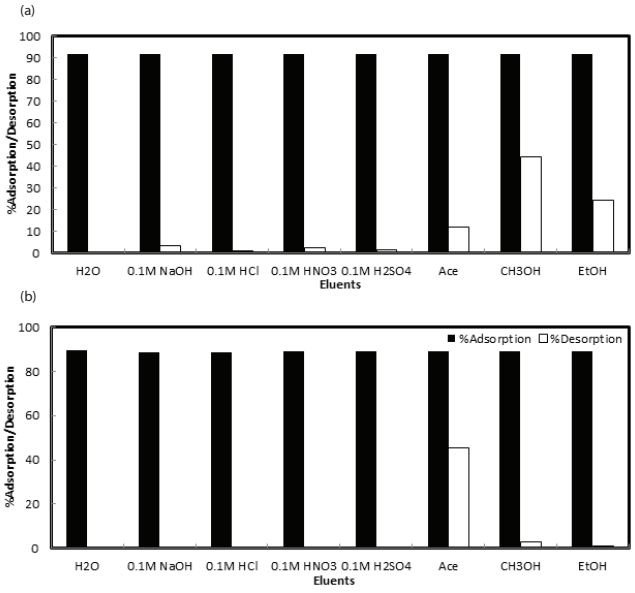

Fig. 7. Adsorption/desorption plots of MG (a) and CV (b) from MCBC.

suggests that the chemical adsorption process might be a major mode of dye removal from MCBC [34].

3.8. Characterization of CBC and MCBC

Fig. 8(a) depicts the XRD pattern of CBC and MCBC. Diffractograms very similar to a characteristic HAP diffractogram [35] were observed, confirming that the compositions of CBC and MCBC were very similar to that of synthetic HAP. The sharp peaks of the diffractogram confirmed that the prepared CBC was crystalline, while a drop in peak intensity after anchoring the dodecyl sulfate to the CBC surface confirmed a decrease in MCBC crystallinity. The surface area analysis data showed a decrease in Brunauer, Emmett, and Teller surface area from 73.176 to 61.963 m^2/g after CBC modification. Adherence of surfactant ions over the CBC surface during modification might be a possible reason for the decrease in surface area. The FT-IR spectra (Fig. 8(b)) showed peaks at 472, 548, 586, and 960 cm^{-1} ascribed to different vibrational modes of the phosphate (PO_4^{3-}) group. Broad bands between 990 and 1,100 cm^{-1} associated with the HPO_4^{2-} group were present in spectra [36]. A low intensity peak at 619 cm^{-1} ascribed to the SO_4^{2-} group [37] appeared in the CBC spectrum; after CBC modification with SDS, the intensity of the peak increased. A peak readily assigned to O–Si–O bending modes appeared at 780 cm^{-1} [38] in the CBC spectrum; it became more intense in the SDS MCBC spectrum and divided into two lobes after MG and CV adsorption. An absorption band characteristic of HAP and associated with the hydroxyl group appeared at 3,570 cm^{-1} [39]. The intensity of this band increased after modification and decreased after MG and CV adsorption. The morphological and elemental composition of CBC and MCBC was assessed by using SEM–EDX. A porous surface with irregular (both spherical and sharp-edged) particle sizes was observed for CBC (Fig. 8(c)). Elemental analysis of CBC confirmed the presence of both Ca and P (major components of HAP) (Fig. 8(d)). The modification of CBC with SDS led to the formation of a nonuniform film over the MCBC surface, resulting in decreased porosity (Fig. 9(a)). The elemental analysis also revealed the presence of S over the MCBC surface, thus confirming the successful adherence of S over the MCBC surface (Fig. 9(b)).

3.9. Adsorption and decoloration mechanism

The proposed dye adsorption mechanism could be described as follows: HAP, the prime component of bone char, has highly active OH^- ions. These ions can be easily replaced by fluoride (F^-) and chloride (Cl^-) ions, producing fluorapatite and chlorapatite. During the modification of CBC with SDS, the surface PO_4^{3-} group of CBC was replaced by the dodecyl sulfate chain of SDS [40]. The OH^- ions present on the MCBC surface provided the major active sites for MG and CV adsorption and were likely responsible for the considerably high adsorption capacity of the synthesized adsorbent. In contrast, the dye molecules (of both MG and CV) possess cationic nitrogen (N) in the form of $–N(CH_3)_2^+$ (Fig. 10, step I) and sp^2-hybridized carbon atoms (Fig. 10, step II). These N- and sp^2-hybridized carbon atoms can easily bind with the –OH group of MCBC through electrostatic interaction and/or a nucleophilic substitution reaction, respectively, leading to the adsorption of dye molecules from an aqueous solution.

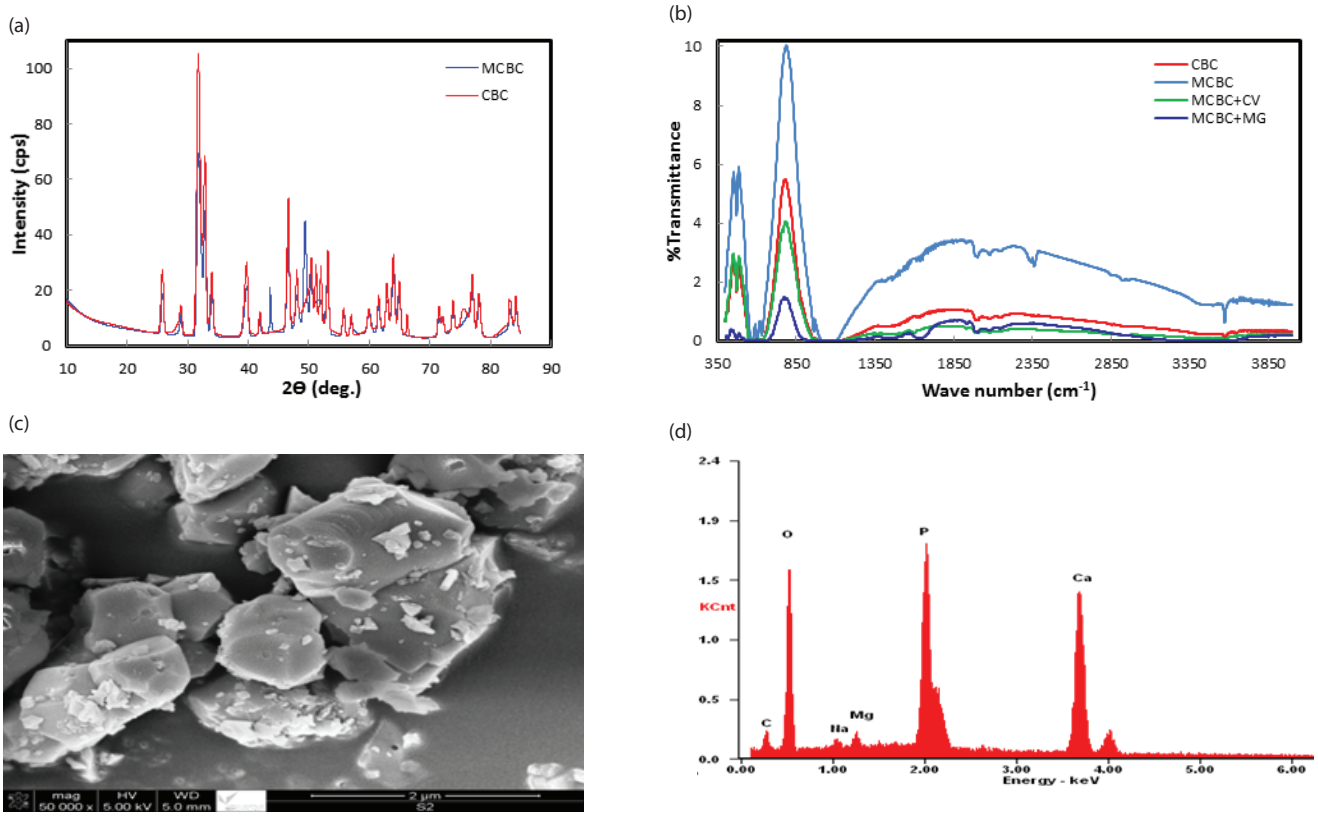

Fig. 8. XRD (a), and FT-IR (b) spectra of CBC and MCBC (before and after dyes adsorption); SEM image (c), and EDX (d) spectrum of CBC.

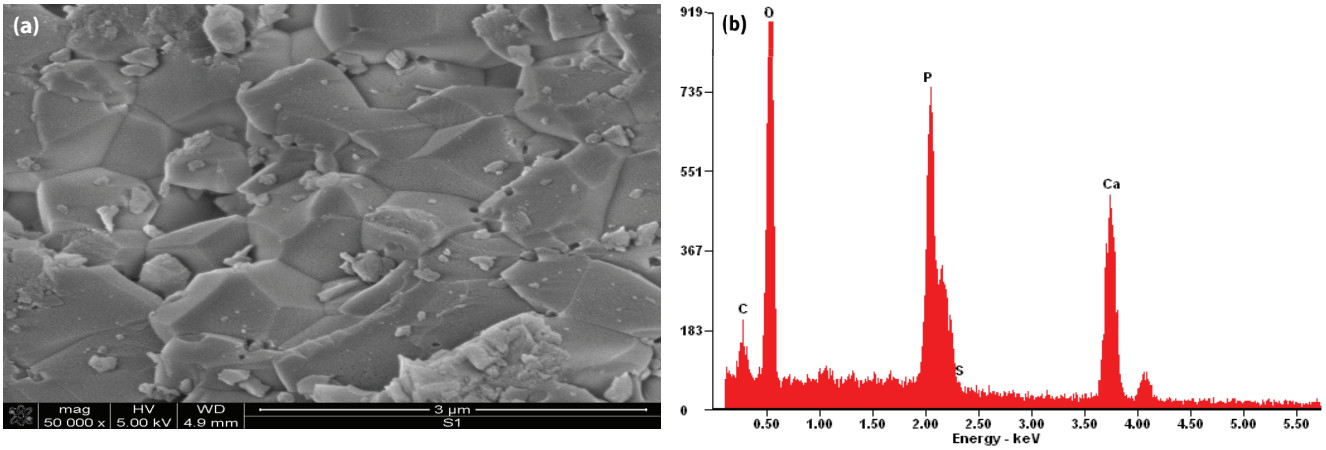

Fig. 9. SEM image (a), and EDX spectra (b) of MCBC.

Taking into account these facts, the proposed dye adsorption mechanisms on MCBC are shown in Fig. 10 (MG) and Fig. 11 (CV). During the pH study, it was observed that at pH < 3, the MCBC does not adsorb cationic dyes because the presence of excess H^+ ions competes with the cationic dyes to adsorb at active sites, but with the increase in pH (pH > 3), the adsorption of cationic dye molecules is favored, most likely due to less competition between the H^+ ion and the cationic dye. Additionally, at lower pH, the H^+ ion can be bonded to the OH^- ion of MCBC, reducing the possibility of its binding with the dyes. On the other hand, the final pH of the solution (after adsorption) shifts toward neutral pH due to the dissociation of OH^- ions of MCBC during the adsorption, which leads to the increase of OH^- ions in the solution. Another possibility for binding dye ions is an electrostatic interaction between the oxygen atom of SDS, introduced over the MCBC surface during the modification step, and the N^+ ion of the dyes. However, it is less favorable due to steric hindrance of the larger-sized dodecyl sulfate anion.

However, the decoloration of residual dyes (after adsorption) with time was also observed (Fig. 12). This can

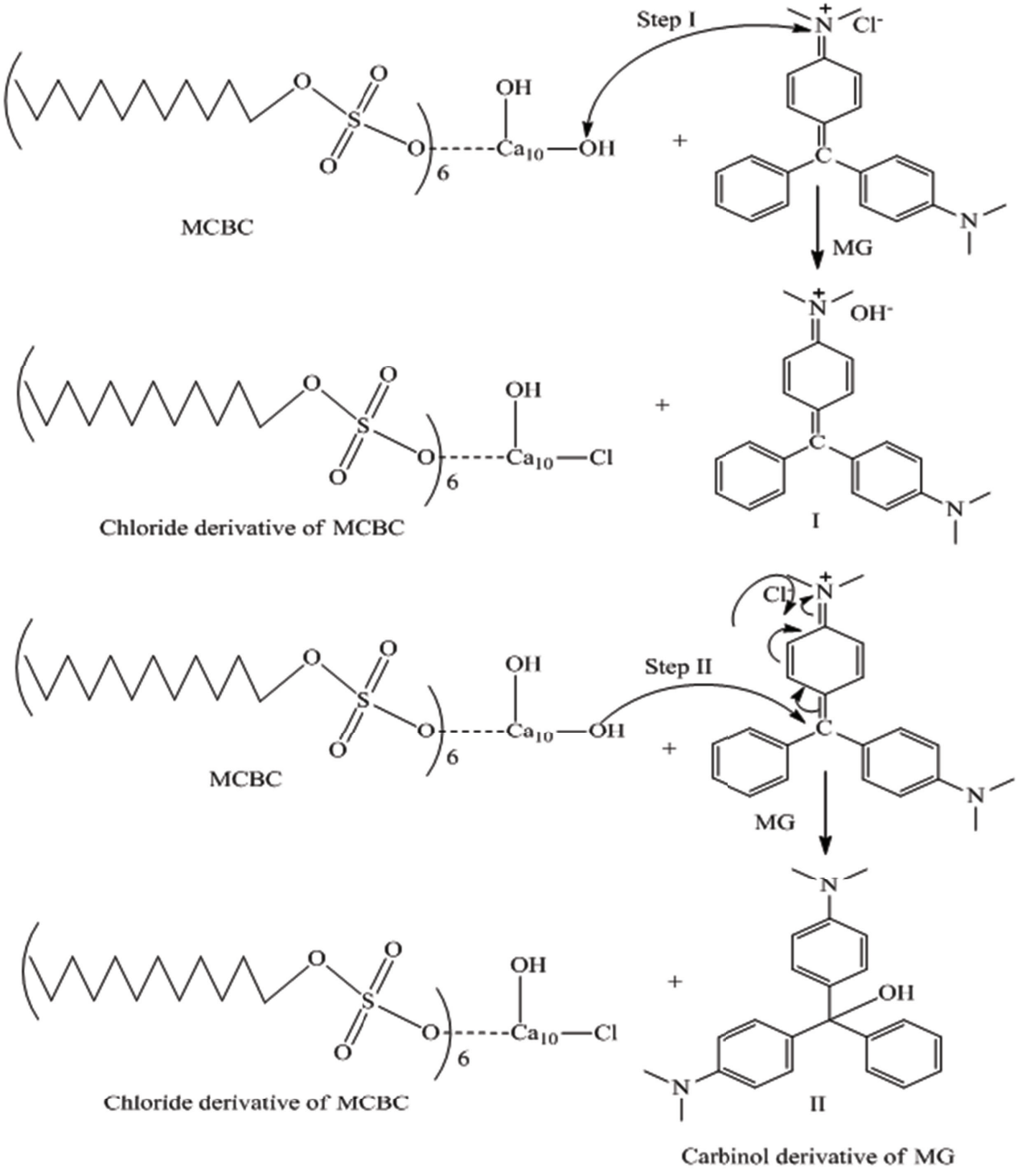

Fig. 10. Possible adsorption/decoloration mechanism of MG on MCBC.

be explained in steps II of Figs. 10 and 11. When the –OH group of MCBC binds with sp^2 carbon atoms of the dyes, the delocalization of π electrons occurs, resulting in the formation of a carbinol derivative for both MG and CV. Thus, the extended π-electron delocalization no longer exists in the cationic dyes, thereby arresting the absorption of visible light, which is responsible for the decoloration of dyes. During the experiment, it was also observed that compared with CV, the decoloration of residual MG was much faster (Fig. 12). This might be because in the carbinol derivative of CV, the extended π-electron delocalization can easily be recreated via the donation of a lone pair of electrons from all three N atoms present in the carbinol derivative of CV (Fig. 11, step III). However, for the carbinol derivative of

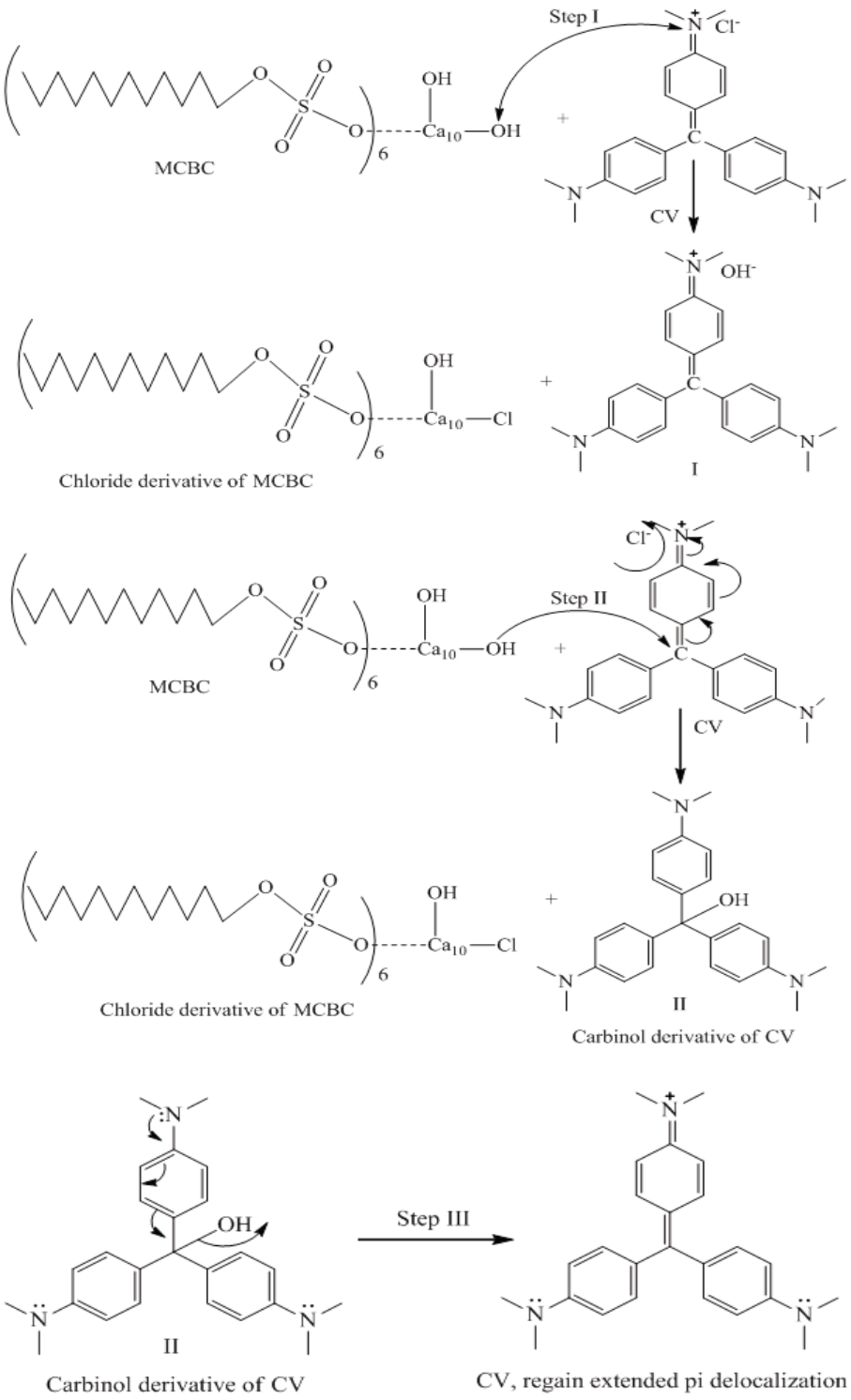

Fig. 11. Possible adsorption/decoloration mechanism of CV on MCBC.

MG, this lone pair donation by N is less favorable than the carbinol derivative of CV. Additionally, the formation of the carbinol derivative of CV after the adsorption on MCBC is difficult compared with MG due to steric hindrance caused by the $-N(CH_3)_2$ groups.

4. Conclusions

Dodecyl sulfate anchored BC from waste camel bones (MCBC) was developed and tested for CV and MG (model adsorbate) removal from the aqueous phase. The maximum

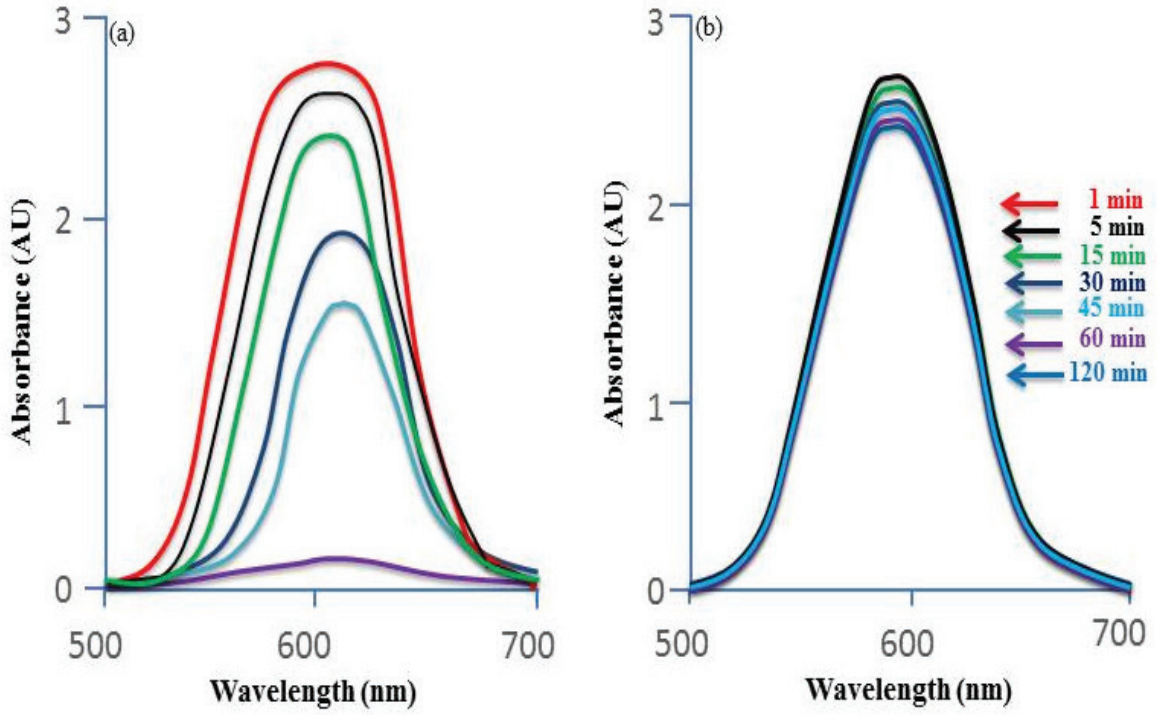

Fig. 12. Effect of time on MG (a) and CV (b) decoloration.

MG (24.94 mg/g) and CV (22.35 mg/g) adsorption was observed at $pH_i > 9$. Adsorption was dependent on adsorbate concentration and temperature. Temkin and Freundlich models showed a better fit for MG and CV, respectively. Comparatively faster adsorption kinetics for MG were observed. Breakthrough capacities in D.I. water, H.A., and T.W. matrices were 2, 2, and 1 mg/g, while exhaustive capacities were 47.5, 30, and 35 mg/g, respectively. Maximum elution occurred using Ace (45.48% MG) and CH_3OH (44.47% CV). Thus, it could be inferred that MCBC is a clean and green adsorbent for the abatement of MG and CV from the aqueous phase, and it would be correct to call it a waste-to-worth approach.

Acknowledgment

The authors would like to extend their sincere appreciation to the Deanship of Scientific Research at King Saud University for funding this work through the Research group No. RG-1437-031.

References

[1] M.T. Yagub, T.K. Sen, S. Afroze, H.M. Ang, Dye and its removal from aqueous solution by adsorption: a review, Adv. Colloid Interface Sci., 209 (2014) 172–184.
[2] M. Yusuf, F.M. Elfghi, S.A. Zaidi, E.C. Abdullah, M.A. Khan, Applications of graphene and its derivatives as an adsorbent for heavy metal and dye removal: a systematic and comprehensive overview, RSC Adv., 5 (2015) 50392–50420.
[3] S. Hosseini, M.A. Khan, M.R. Malekbala, W. Cheah, T.S.Y. Choong, Carbon coated monolith, a mesoporous material for the removal of methyl orange from aqueous phase: adsorption and desorption studies, Chem. Eng. J., 171 (2011) 1124–1131.
[4] J.A. Wilson, I.D. Pulford, S. Thomas, Sorption of Cu and Zn by bone charcoal, Environ. Geochem. Health, 25 (2003) 51–56.
[5] L. Pivarčiová, O. Rosskopfová, M. Galamboš, P. Rajec, Adsorption behavior of Zn(II) ions on synthetic hydroxyapatite, Desal. Wat. Treat., 55 (2015) 1825–1831.
[6] N. Barka, K. Ouzaouit, M. Abdennouri, M. El Makhfouk, S. Qourzal, A. Assabbane, Y. Ait-Ichou, A. Nounah, Kinetics and equilibrium of cadmium removal from aqueous solutions by sorption onto synthesized hydroxyapatite, Desal. Wat. Treat., 43 (2012) 8–16.
[7] K. Mahmud, Md. A. Islam, A. Mitsionis, T. Albanis, T. Vaimakis, Adsorption of direct yellow 27 from water by poorly crystalline hydroxyapatite prepared via precipitation method, Desal. Wat. Treat., 41 (2012) 170–178.
[8] W.G. Kim, M.N. Kim, S.M. Lee, J.K. Yang, Removal of Cu(II) with hydroxyapatite (animal bone) as an inorganic ion exchanger, Desal. Wat. Treat., 4 (2009) 269–273.
[9] D. Uzunoğlu, A. Özer, Adsorption of Acid Blue 121 dye on fish (*Dicentrarchus labrax*) scales, the extracted from fish scales and commercial hydroxyapatite: equilibrium, kinetic, thermodynamic, and characterization studies, Desal. Wat. Treat., 57 (2016) 14109–14131.
[10] M.A. Al-Ruwaili, O.M. Khalil, S.A. Selim, Viral and bacterial infections associated with camel (*Camelus dromedarius*) calf diarrhea in North Province, Saudi Arabia, Saudi J. Biol. Sci., 19 (2012) 35–41.
[11] E.A.M. Hamam, Effect of Roughages on Growth Rate and Feed Conversion in Young Camels, MSc Thesis, King Saud University, Riyadh, Saudi Arabia, 1993.
[12] B. Samiey, A.R. Toosi, Kinetics study of malachite green fading in the presence of TX 100, DTAB and SDS, Bull. Korean Chem. Soc., 30 (2009) 2051–2056.
[13] S. Shimabayashi, H. Tanaka, M. Nakagaki, Effect of added salt on the adsorption of dodecyl sulfate ion and concurrent release of phosphate and calcium ions at the surface of hydroxyapatite, Chem. Pharm. Bull., 35 (1987) 2171–2176.
[14] X. Pan, J. Wang, D. Zhang, Sorption of cobalt to bone char: kinetics, competitive sorption and mechanism, Desalination, 249 (2009) 609–614.
[15] I.D. Smičiklasa, S.K. Milonjića, P. Pfendt, S. Raičevića, The point of zero charge and sorption of cadmium (II) and strontium (II)

ions on synthetic hydroxyapatite, Sep. Purif. Technol., 18 (2000) 185–194.
[16] K.-S. Low, C.-K. Lee, B.-F, Tan, Quaternized wood as sorbent for reactive dyes, Appl. Biochem. Biotechnol., 87 (2000) 233–245.
[17] L. Zhang, H. Zhang, W. Guo, Y. Tian, Removal of malachite green and crystal violet cationic dyes from aqueous solution using activated sintering process red mud, Appl. Clay Sci., 93–94 (2014) 85–93.
[18] I. Langmuir, The adsorption of gases on plane surface of glass, mica and platinum, J. Am. Chem. Soc., 40 (1916) 1361–1403.
[19] H.M.F. Freundlich, Over the adsorption in solution, J. Phys. Chem., 57 (1906) 385–470.
[20] M.I. Tempkin, V. Pyzhev, Kinetics of ammonia synthesis on promoted iron catalyst, Acta Phys. Chim. USSR, 12 (1940) 327–356.
[21] S. Chowdhury, S. Chakraborty, P.D. Saha, Removal of crystal violet from aqueous solution by adsorption onto eggshells: equilibrium, kinetics, thermodynamics and artificial neural network modeling, Waste Biomass Valori., 4 (2013) 655–664.
[22] K. Porkodi, K.V. Kumar, Equilibrium, kinetics and mechanism modeling and simulation of basic and acid dyes sorption onto jute fiber carbon: eosin yellow, malachite green and crystal violet single component systems, J. Hazard. Mater., 143 (2007) 311–327.
[23] V.K. Garg, R. Kumar, R. Gupta, Removal of malachite green dye from aqueous solution by adsorption using agro-industry waste: a case study of *Prosopis cineraria*, Dyes Pigm., 62 (2004) 1–10.
[24] S.D. Khattri, M.K. Singh, Removal of malachite green from dye wastewater using neem sawdust by adsorption, J. Hazard. Mater., 167 (2009) 1089–1094.
[25] B.H. Hameed, M.I. El-Khaiary, Malachite green adsorption by rattan sawdust: isotherm, kinetic and mechanism modeling, J. Hazard. Mater., 159 (2008) 574–579.
[26] S. Chakraborty, S. Chowdhury, P.D. Saha, Adsorption of Crystal Violet from aqueous solution onto NaOH-modified rice husk, Carbohydr. Polym., 86 (2011) 1533–1541.
[27] R. Ahmad, R. Kumar, Adsorption studies of hazardous malachite green onto treated ginger waste, J. Environ. Manage., 91 (2010) 1032–1038.
[28] A. Saeed, M. Sharif, M. Iqbal, Application potential of grapefruit peel as dye sorbent: kinetics, equilibrium and mechanism of crystal violet adsorption, J. Hazard. Mater., 179 (2010) 564–572.
[29] S. Lagergren, About the theory of so-called adsorption of soluble substances, K. Sven. Vetenskapsakad. Handl., 24 (1898) 1–39.
[30] Y.S. Ho, G. McKay, The kinetics of sorption of divalent metal ions onto sphagnum moss peat, Water Res., 34 (2000) 735–742.
[31] M.A. Khan, M. Ngabura, T.S.Y. Choong, H. Masood, L.A. Chuah, Biosorption and desorption of nickel on oil cake: batch and column studies, Bioresour. Technol., 103 (2012) 35–42.
[32] R.A.K. Rao, M.A. Khan, Removal and recovery of Cu(II), Cd(II) and Pb(II) ions from single and multimetal systems by batch and column operation on neem oil cake (NOC), Sep. Purif. Technol., 57 (2007) 394–402.
[33] M.C. Brum, J.F. Oliveira, Removal of humic acid from water by precipitate flotation using cationic surfactants, Mineral Eng., 20 (2007) 945–949.
[34] A.R. Nesic, S.J. Velickovic, D.G. Antonovic, Novel composite films based on amidated pectin for cationic dye adsorption, Colloids Surf., B, 116 (2014) 620–626.
[35] G. Ciobanu, M. Harja, M. Diaconu, C. Cimpeanu, R. Teodorescu, D. Bucur, Crystal violet dye removal from aqueous solution by nanohydroxyapatite, J. Food Agric. Environ., 12 (2014) 499–502.
[36] I. Smičiklas, S. Dimović, I. Plećaš, M. Mitrić, Removal of Co^{2+} from aqueous solutions by hydroxyapatite, Water Res., 40 (2006) 2267–2274.
[37] S.K. Verma, M.K. Deb, Direct and rapid determination of sulphate in environmental samples with diffuse reflectance Fourier transform infrared spectroscopy using KBr substrate, Talanta, 71 (2007) 1546–1552.
[38] S.N. Cesaro, C. Lemorini, The function of prehistoric lithic tools: a combined study of use-wear analysis and FTIR microspectroscopy, Spectrochim. Acta, Part A, 86 (2012) 299–304.
[39] Y.-N. Chen, L.-Y Chai, Y.-D. Shu, Study of arsenic(V) adsorption on bone char from aqueous solution, J. Hazard. Mater., 160 (2008) 168–172.
[40] S. Shimabayashi, N. Hashimoto, H. Kawamura, T. Uno, Formation of Hydroxyapatite in the Presence of Phosphorylated and Sulfated Polymer in an Aqueous Phase, A. Zahid, Ed., Mineral Scale Formation and Inhibition, Plenum Press, New York, 1995.